Published by Institute of Physics Publishing for SISSA/ISAS
Received: *October 7, 2004*
Accepted: *November 9, 2004*

Closed bosonic string field theory at quartic order

Nicolas Moeller

Department of Mathematics, King's College London
London, WC2R 2LS, U.K.
E-mail: moeller@mth.kcl.ac.uk

Abstract: We give a complete numerical description of the geometry of the four-point contact interaction of closed bosonic string field theory. Namely, we compute the boundary of the relevant region of the moduli space of the four-punctured spheres, and everywhere in this region we give the local coordinates around each punctures in terms of a Strebel quadratic differential and mapping radii. The numerical methods are explained in details. And the results are translated into fits, which can in principle be used to compute the contact interaction of any four off-shell string states.

Keywords: Bosonic Strings, String Field Theory.

JHEP11(2004)018

Contents

1. Introduction

Although a field theory of closed bosonic strings is known ([1]–[3]), until now only very little progress has been made in understanding the fate of the bulk tachyon of the closed bosonic string theory. Yet, calculating the tachyon potential, and rewriting the theory around one of its minimum, is probably the first thing that one should do if one is given a field theory with a tachyonic instability. The problem with closed bosonic string field theory (CSFT) is its complexity; unlike open string field theory, which is cubic in the string field, CSFT is non-polynomial. This adds a great deal of complexity, because all terms higher than cubic will involve an integration over a subset of the moduli space of the relevant Riemann surfaces; and at every point of this restricted moduli space we need to specify local coordinates, so that we can properly insert the off-shell vertex operators.

It may be nevertheless feasible to do calculations in CSFT, by truncating the action to some finite polynomial order; it is possible that the results computed from the truncated action converge as the truncation order is increased. If we can do so, one of the most important questions that we would like to answer, is whether the tachyon potential has a minimum or not. If it has a global minimum, then it is natural to expect that the theory expanded around this minimum may be a superstring theory. The mechanism by which the bosonic theory would flow to a superstring theory by tachyon condensation, would have to involve spontaneous breaking of the twenty-six dimensional Poincaré symmetry. Evidence that this can happen in CSFT at low order, was given in [4]. This is also supported by the fact that all the ten-dimensional superstring theories can be realized from the closed bosonic string theory after some suitable compactification and truncation of the spectrum ([5]). But although the tachyon potential has a minimum to third order in the string field (as was originally found in [6]), to quartic order it doesn't have a minimum anymore, as was shown in [7]. Clearly, to get some new insight into this question, we need to express the tachyon potential to higher orders.

Another interesting question, which has appeared more recently in the literature (see [8, 9] and references therein), is that of the condensation of closed tachyons localized on the apex of an orbifold. It has been conjectured that the condensation of such tachyons changes the background geometry to that of an orbifold with a lesser deficit angle, until it eventually condenses to flat space. A numerical check of this conjecture was attempted in [9] in closed bosonic string theory. At low order and truncation level, a relatively good agreement (of roughly 70%) was found. Here too, a more thorough study of the problem is very likely to require contact interactions of higher orders.

In [7], Belopolsky calculated the four-tachyon contact term. His method relied on analytical properties of the quadratic differentials on a four-punctured sphere (although numerical computations were still needed in order to extract the amplitude). Unfortunately, these analytical methods don't seem to generalize obviously to the contact interactions of more than four strings. The goal of the present paper is to provide an efficient numerical method for calculating the geometry of the contact interactions, that does generalize to higher order interactions. We also give our numerical results, that describe completely the geometry of the interaction everywhere in the moduli space. They can thus be used to calculate the contact amplitude of any four off-shell string states.

The structure of the paper is as follows: first, in section 2, we briefly review how to calculate the contact amplitudes with the help of quadratic differentials, and how the local coordinates at the punctures can be computed from the Strebel quadratic differential. We review the moduli space of the contact interaction in section 3. In section 4, we expose in details our numerical method to find the Strebel differential at a given point in the moduli space; then we go on and describe, in section 5, our numerical method to compute the mapping radii of the Strebel differential. We then present our numerical results in section 6, in the form of fits. And in section 7, we show that the result of [7] for the four-tachyon contact term is confirmed by our results. Finally, section 8 is devoted to discussions and conclusions.

2. The geometry of the contact interaction

In this section, we summarize very briefly the notions that are necessary to compute off-shell contact amplitudes. More detailed explanations can be found in [2, 7, 10, 11].

JHEP11(2004)018

To calculate an off-shell contact amplitude of N string states on an N-punctured sphere, one must insert the vertex operators at the punctures, transforming them according to the local coordinates at the punctures. One then calculates their correlation function after inserting antighosts. At last, one has to integrate the correlators on the relevant subset[1] $\mathcal{V}_{0,N}$ of the moduli space of N-punctured spheres. The geometry of the punctured sphere that determines the local coordinates at the punctures, is given by the metric of minimal area[2] with the constraint that every nontrivial closed curve has length $\geq 2\pi$. It follows that the geometry of the punctured sphere is that of N semi-infinite cylinders of circumference 2π, joining along the edges of a polyhedron whose vertices always join three edges. The constraint on the nontrivial closed curves ensures that we do not over-count Feynman diagrams. The solution to this minimal area metric is given by a Strebel quadratic differential, which we now briefly introduce.

A quadratic differential φ is a geometrical object that lives on a Riemann surface. In the local coordinate z, it takes the form $\varphi = \phi(z)(dz)^2$; and it is invariant under conformal changes of local coordinates, in the sense that, if w is another coordinate, we have

$$\phi(z)(dz)^2 = \phi(w)(dw)^2 . \tag{2.1}$$

A quadratic differential defines a metric, whose length element is $ds = \sqrt{|\phi(z)|}\,|dz|$. In particular, in a neighborhood of a second order pole $z = p$,

$$\phi(z) = \frac{r}{(z-p)^2} + \mathcal{O}\left((z-p)^{-1}\right) , \tag{2.2}$$

and if $r < 0$, the geometry is that of a semi-infinite cylinder of circumference $-2\pi r$. The quadratic differentials that we will consider here are regular everywhere except at the punctures, where they have second order poles. We will call the quantity r in (2.2), the *residue* of φ at the puncture p. It is easy to see from (2.1), that the notions of pole and of residue, as well as the zeros of φ, are conformal invariants. If φ has a second order pole with residue r at $z = p$, then there is a local coordinate w, defined in a neighborhood of the puncture, in which

$$\varphi = \frac{r}{w^2}(dw)^2 . \tag{2.3}$$

We will call such a local coordinate w, a *natural coordinate* at the puncture $z = p$.

A *horizontal trajectory* of φ is a maximal curve on which $\phi(z)(dz)^2 > 0$, where dz is tangential to the curve. For example, the horizontal trajectories of (2.3) are circles centered at the puncture $w = 0$. A *critical* horizontal trajectory is a horizontal trajectory one of whose ends is either a zero or a pole of order one. We note here that, as one can easily verify, a zero of order n is the source of $n + 2$ horizontal trajectories. The *critical graph* of φ is the set formed by all critical horizontal trajectories.

[1]In general $\mathcal{V}_{g,N}$ is the restricted moduli space of the N-punctured Riemann surfaces of genus g. Although we will consider here only the case $g = 0$, we will keep this notation.

[2]Actually, since in our case the area is infinite, we have to minimize the *reduced* area. See [3] for more details.

JHEP11(2004)018

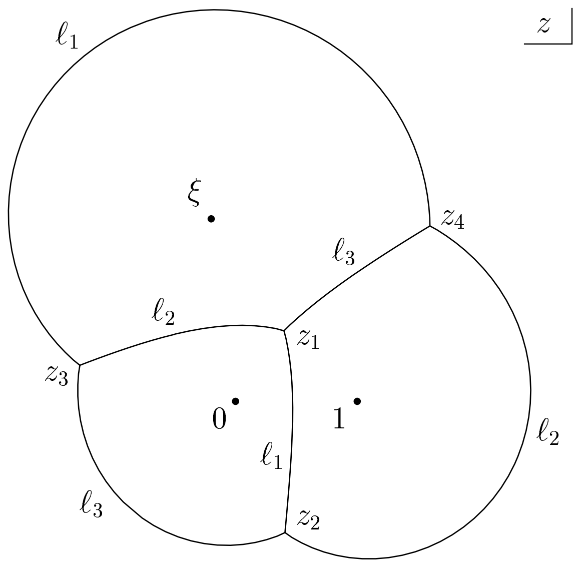

Figure 1: The critical graph of the Strebel differential, whose poles are at 0, 1, ξ, and ∞; here we have chosen the particular value $\xi = -0.2 + 1.5\,i$. It has the topology of a tetrahedron, with a puncture on each side. Its zeros are labelled z_i, $i = 1, \ldots, 4$. We have also labelled the edge lengths ℓ_i (note that two opposite edges have the same length).

From now on, we will only consider the case of the 4-punctured spheres, which we will describe in the uniformizer coordinate z. The last definition[3] that we need is that of the *Strebel differential*. It is a quadratic differential whose four poles are second order poles with residue -1, and whose critical graph has the topology of a tetrahedron. In particular, the Strebel differential has four simple zeros, which are the vertices of the tetrahedron, at which three critical trajectories (edges) are joining. See figure 1 for the critical graph of a particular Strebel differential. On this figure we have also labelled the lengths (in the φ-metric) of the edges of the tetrahedron. From the residue conditions, it is easy to see that two opposite edges (which don't touch each other) have the same length. Also we have that the circumference of each face is 2π, in particular $\ell_1 + \ell_2 + \ell_3 = 2\pi$, and thus we have only two independent lengths, for example ℓ_1 and ℓ_2.

Using the $\mathrm{PSL}(2,\mathbb{C})$ automorphism group of the Riemann sphere, we can always place three punctures at, respectively, $z = 0$, 1, and ∞. The fourth puncture will be called ξ. The residue condition for the Strebel differential, is satisfied by the general form

$$\begin{aligned} \phi(z) &= \frac{-(z^2-\xi)^2}{z^2\,(z-1)^2\,(z-\xi)^2} + \frac{a}{z\,(z-1)\,(z-\xi)} \\ &= \frac{-z^4 + a\,z^3 + (2\xi - (1+\xi)a)\,z^2 + a\xi\,z - \xi^2}{z^2\,(z-1)^2\,(z-\xi)^2}\,, \end{aligned} \tag{2.4}$$

[3]This definition can be made much more general, but for simplicity, we restrict ourselves here to the four-punctured spheres.

where a is any complex number. The puncture conditions at 0, 1 and ξ are straightforwardly verified from the above form. For the puncture at infinity, we need to change the coordinate to $w = 1/z$, and we should verify that $\phi(w) = -1/w^2 + \mathcal{O}(w^{-1})$. This is easily done:

$$\begin{aligned}
\phi(z)(dz)^2 &= \phi(w)(dw)^2 \\
\Rightarrow \phi(w) &= \phi\left(z = \frac{1}{w}\right)\left(\frac{dz}{dw}\right)^2 = \phi\left(z = \frac{1}{w}\right)\frac{1}{w^4} = -\frac{1}{w^2} + \mathcal{O}(w^{-1}),
\end{aligned}$$

where by $\phi(z = 1/w)$ we mean the function $\phi(z)$ in the coordinate z, evaluated at $z = 1/w$. And we see that (2.4) is therefore the most general form satisfying the residue condition.

The metric defined from the Strebel differential is a metric of minimal area. Moreover, by a theorem of Strebel ([11]), the Strebel differential for a given ξ is unique. Therefore, if all nontrivial closed curves on the punctured sphere, have length $\geq 2\pi$, we will have solved our minimal area problem. One of the results of this paper is to determine numerically the coefficient a in (2.4), and therefore φ, for all values of ξ in the restricted moduli space.

The Strebel differential defines (up to unimportant phases) the conformal maps from the four punctured disks (with local natural coordinates w_n) to a 4-punctured sphere, in such a way that the punctures $w_n = 0$ are mapped to the punctures $z = p_n$, and the boundaries $|w_n| = 1$ of the unit disks are mapped to the part of the critical graph surrounding p_n (see figure 2). Our notation is that the punctures are labelled by the index n running from 1 to 4, with $p_1 = 0$, $p_2 = 1$, $p_3 = \xi$ and $p_4 = \infty$. The method for expressing explicitly these conformal maps from the knowledge of φ was described in [10]. First, we expand φ in a Laurent series around the puncture p_n.

$$\varphi = \left(-\frac{1}{(z-p_n)^2} + \frac{b_{-1}}{z-p_n} + b_0 + b_1(z-p_n) + \cdots\right)(dz)^2 . \tag{2.5}$$

The coefficients b_i are calculated straightforwardly from (2.4). The map from the punctured unit disk to the punctured sphere, is expanded as follows[4]

$$z = h_n(w_n) = p_n + (\rho_n w_n) + d_1\,(\rho_n w_n)^2 + d_2\,(\rho_n w_n)^3 + \cdots . \tag{2.6}$$

Here $\rho_n = |\frac{dz}{dw_n}|_{w_n=0}$ is the *mapping radius* of the conformal map h_n. In the natural coordinates w_n, the quadratic differential has the form

$$\varphi = -\frac{1}{w_n^2}(dw_n)^2 . \tag{2.7}$$

Now we use (2.5), (2.6) and (2.7) to calculate recursively the coefficients d_i from the b_i's. For the first few coefficients, we get

$$d_1 = \frac{1}{2}b_{-1}$$

[4]Our notation here differs from [10]. It is convenient to expand in powers of $(\rho_n w_n)$, instead of w_n.

JHEP11(2004)018

$$
\begin{aligned}
d_2 &= \frac{1}{16}\left(7\,b_{-1}{}^2 + 4\,b_0\right) \\
d_3 &= \frac{1}{48}\left(23\,b_{-1}{}^3 + 28\,b_{-1}b_0 + 8\,b_1\right) \\
d_4 &= \frac{1}{768}\left(455\,b_{-1}{}^4 + 856\,b_{-1}{}^2 b_0 + 144\,b_0{}^2 + 368\,b_{-1}b_1 + 96\,b_2\right)\,. \\
&\ \vdots
\end{aligned}
$$

Note that the mapping radii cannot be calculated from the above recursive method. But they can be calculated, for example, by the formula (5.1) derived in [10]. As a consistency check of our results, we have calculated the conformal maps as a series (2.6) to order 18, for the particular value $\xi = -0.2 + 1.5\,i$. We find $a = 1.12245 + 1.23948\,i$, and

$$
\begin{aligned}
\rho_1 &= 0.69819 \\
\rho_2 &= 0.88628 \\
\rho_3 &= 1.34118 \\
\rho_4 &= 0.46138\,.
\end{aligned}
$$

In figure 2, we have represented the four conformal maps by mapping circles of radii $k/10$ for $k = 1, \ldots, 10$.

3. The moduli space

As already mentioned, a point ξ belongs to the moduli space $\mathcal{V}_{0,4}$ of the contact interaction (also called *restricted* moduli space), only if all nontrivial closed curves on its corresponding tetrahedron have length $\geq 2\pi$. One can easily check that this is equivalent to the conditions

$$\ell_1,\, \ell_2,\, \ell_3 \leq \pi\,, \tag{3.1}$$

where the ℓ_i are the edge lengths (see figure 1). We show $\mathcal{V}_{0,4}$ in figure 3. It is delimited by three curves $\mathcal{B}_1$, $\mathcal{B}_2$ and $\mathcal{B}_3$ on which, respectively ℓ_1, ℓ_2 and ℓ_3 are equal to π.

We don't need to calculate the Strebel differential everywhere on this space because there are some symmetries. First, there is the obvious symmetry $\xi \to \xi^*$. Then there are six $\mathrm{PSL}(2,\mathbb{C})$ transformations that permute the three fixed poles $\{0, 1, \infty\}$. They are generated by

$$g_1: \quad \xi \to 1 - \xi \tag{3.2}$$

$$\text{and} \qquad g_2: \quad \xi \to \frac{1}{\xi}\,. \tag{3.3}$$

In total, $\mathcal{V}_{0,4}$ is thus made of twelve parts separated by the real axis, the line $\mathrm{Re}(\xi) = 1/2$, and two circles of unit radius centered on 0 and on 1 respectively. In our computations, we will therefore only consider the subspace $\mathcal{A}$, which is bounded from the right by $\{\xi : \mathrm{Re}(\xi) = 1/2\}$, from below by the unit circle centered on 0, and from the left and the top by the curve $\mathcal{B}_1$ (see figure 3).

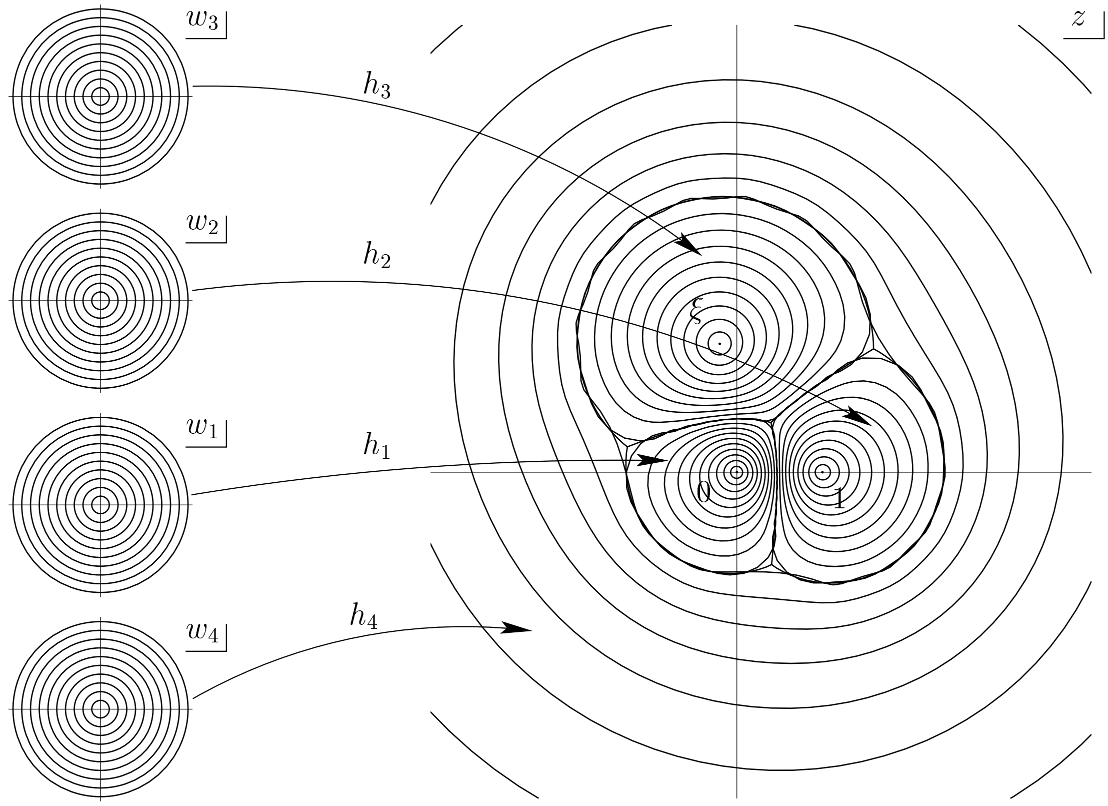

Figure 2: The four conformal maps as series (2.6) to order 18, are represented for the particular value $\xi = -0.2 + 1.5\,i$ by mapping circles of radii $k/10$ for $k = 1, \ldots, 10$. Also plotted is the critical graph of the quadratic differential.

To find the parameter a in the other regions of $\mathcal{V}_{0,4}$, we apply, for $\mathrm{PSL}(2,\mathbb{C})$ transformations $\xi \to g(\xi)$, the transformation law (2.1) to φ given in (2.4); and when $\xi \to \xi^*$, we have $a \to a^*$. The transformation law for the mapping radius ρ_n at the puncture p_n, is

$$\rho_n \to \left|g'(p_n)\right| \, \rho_n \,. \tag{3.4}$$

And it is invariant under complex conjugation $\xi \to \xi^*$. Note that if g in (3.4), sends the finite puncture p_n to infinity, one must calculate its transformation in the coordinate $w = 1/z$. In particular, if $g(\xi) = 1/\xi$, the mapping radii at the punctures $z = 0$ and $z = \infty$ are invariant.

Note that we don't know the analytic expressions of the curves $\mathcal{B}_i$. We thus have to calculate one of them, say $\mathcal{B}_1$, numerically. This is done by finding the points where $\ell_1 = \pi$; the result will be presented in section 6. But we can already understand a few points of this moduli space. First, when $\xi = 1/2$, we can show that the Strebel differential is given by $a = 2$, and then one can verify that $\ell_2 = \ell_3 = \pi$. This shows that at the point $\xi = 1/2$, the two curves $\mathcal{B}_2$ and $\mathcal{B}_3$ intersect. And therefore, from the symmetry of $\mathcal{V}_{0,4}$, one also has that, at $\xi = -1$, $\mathcal{B}_1$ and $\mathcal{B}_2$ intersect, while at $\xi = 2$, it is $\mathcal{B}_1$ and $\mathcal{B}_3$ that intersect. The knowledge that the point $\xi = -1$ belongs to $\mathcal{B}_1$, will be used in section 6, when we express

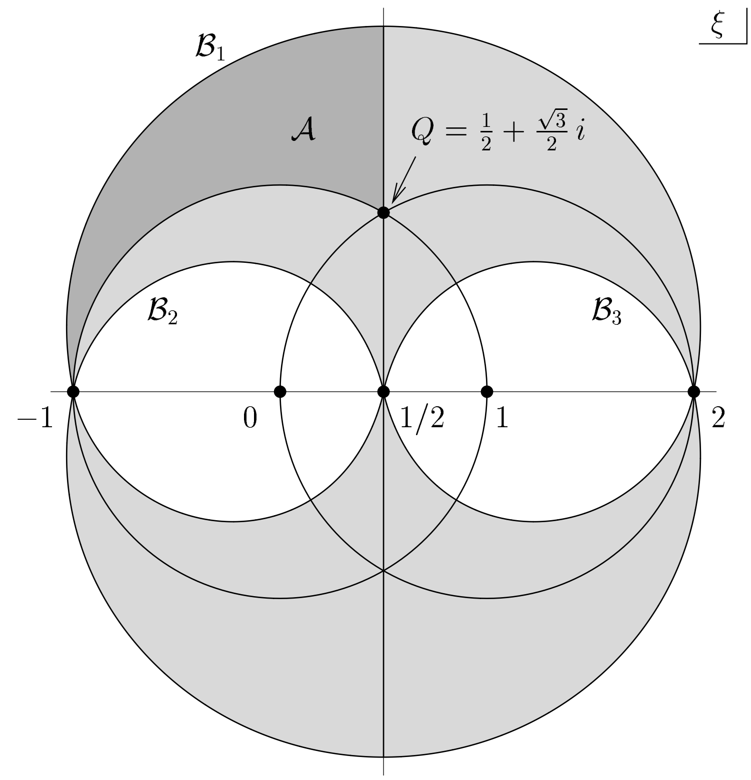

Figure 3: The moduli space $\mathcal{V}_{0,4}$. It is bounded by the three curves $\mathcal{B}_1$, $\mathcal{B}_2$ and $\mathcal{B}_3$. We need only to concentrate on the space $\mathcal{A}$ (shaded in darker grey), bounded by $\mathcal{B}_1$, the unit circle at the origin, and the line $\mathrm{Re}\, z = 1/2$; all the other regions can be reached from $\mathcal{A}$ by $\mathrm{PSL}(2, \mathbb{C})$ transformations and complex conjugations.

$\mathcal{B}_1$ as a fit. Note that all these points on the real axis are singular, in the sense that the Strebel differentials at those points have double zeros, which means that the tetrahedron is singular, two of its edges having collapsed to zero length.

The point $Q \equiv \frac{1}{2} + \frac{\sqrt{3}}{2}\, i$ is also interesting. Indeed, when $\xi = Q$, the three punctures 0, 1 and ξ are placed at the corners of an equilateral triangle. In fact, this is the most symmetric configuration, whose corresponding tetrahedron is a regular tetrahedron. One can check that for this configuration, $a = 2 + \frac{2}{\sqrt{3}}\, i$.

4. Computation of the Strebel differential

Here we explain in details how to find the parameter a in (2.4) such that the quadratic differential is the Strebel differential for the specified position of the fourth puncture ξ. Once a is found, the mapping radii can be computed relatively easily; this will be described in the next section. The numerical results for a and the mapping radii will be presented in section 6.

We define the *complex length* of a curve C by $\ell(C) \equiv \int_C \sqrt{\phi(z)} dz$ or, if C is a segment from z_i to z_j,

$$\ell(z_i, z_j) \equiv \int_{z_i}^{z_j} \sqrt{\phi(z)}dz\,. \tag{4.1}$$

The square root must be chosen such that its branch cut doesn't intersect the path of integration. Now suppose that z_i and z_j are zeros of φ, and that φ is the Strebel differential. This means that there is a critical trajectory, that we call C, joining z_i and z_j. From the definition of a horizontal trajectory, we have that $\sqrt{\phi(z)}dz$ is real on C, and therefore $\ell(C)$ is real (and is equal to the length of C in the φ-metric). By deforming the path of integration, we then have that $\ell(z_i, z_j)$ is real. Indeed, even if φ has a pole in between C and the segment $[z_i, z_j]$, the residue of this pole would change the integral only by a real quantity, because the residues (in the usual sense) of $\sqrt{\phi(z)}$ are all purely imaginary.

Therefore, in order to find the Strebel differential, we will look for the quadratic differential φ that satisfies the condition that $\ell(z_i, z_j)$ must be real for any two zeros z_i and z_j. Since the quadratic differentials (2.4) that we are considering, are already constrained to have residues -1 at the four punctures, we easily see that the above reality condition is satisfied if $\ell(z_i, z_j)$ is real for two independent segments; for example

$$\begin{cases} \operatorname{Im} \ell(z_1, z_2) = 0 \\ \operatorname{Im} \ell(z_1, z_3) = 0\,, \end{cases} \tag{4.2}$$

where z_1, z_2 and z_3 are three zeros of φ. Solving these two real equations will determine the complex parameter a.

To solve the system of equations (4.2), we use the Newton method in two dimensions. Namely, we have two real equations for the two real unknowns $\operatorname{Re} a$ and $\operatorname{Im} a$. In general, the Newton method for the system of n equations of n unknowns $\vec{f}(\vec{x}) = 0$ consists of starting with a $\vec{x}_0$ not too far from the solution, and repeating the iteration

$$\vec{x}_{i+1} = \vec{x}_i - J(\vec{x}_i)^{-1}\vec{f}(\vec{x}_i)$$

until $\vec{x}_i$ converges. Here $J(\vec{x}_i) = (\frac{\partial \vec{f}}{\partial \vec{x}})_{\vec{x}=\vec{x}_i}$ is the jacobian. In order to calculate it in our situation, we note that for a holomorphic function $f(z)$ we have $\frac{\partial \operatorname{Im} f(z)}{\partial \operatorname{Re} z} = \operatorname{Im} f'(z)$, and $\frac{\partial \operatorname{Im} f(z)}{\partial \operatorname{Im} z} = \operatorname{Re} f'(z)$. Our jacobian is thus

$$J = \begin{pmatrix} \frac{\partial \operatorname{Im} \ell(z_1,z_2)}{\partial \operatorname{Re} a} & \frac{\partial \operatorname{Im} \ell(z_1,z_2)}{\partial \operatorname{Im} a} \\ \frac{\partial \operatorname{Im} \ell(z_1,z_3)}{\partial \operatorname{Re} a} & \frac{\partial \operatorname{Im} \ell(z_1,z_3)}{\partial \operatorname{Im} a} \end{pmatrix} = \begin{pmatrix} \operatorname{Im} \frac{d}{da}\ell(z_1, z_2) & \operatorname{Re} \frac{d}{da}\ell(z_1, z_2) \\ \operatorname{Im} \frac{d}{da}\ell(z_1, z_3) & \operatorname{Re} \frac{d}{da}\ell(z_1, z_3) \end{pmatrix}, \tag{4.3}$$

and we will need therefore to evaluate $\frac{d}{da}\ell(z_i, z_j)$ as well as $\ell(z_i, z_j)$.

But before we go on and solve the system of equations (4.2), we see that there is a problem with the computation of the complex lengths (4.1), namely we need a square root whose branch cut we shall never intersect, although we have to evaluate it along various paths whose positions we don't know *à priori.* The solution to this problem, a square root without a branch cut, is a central tool of our numerical methods; it is presented in the next subsection.

JHEP11(2004)018

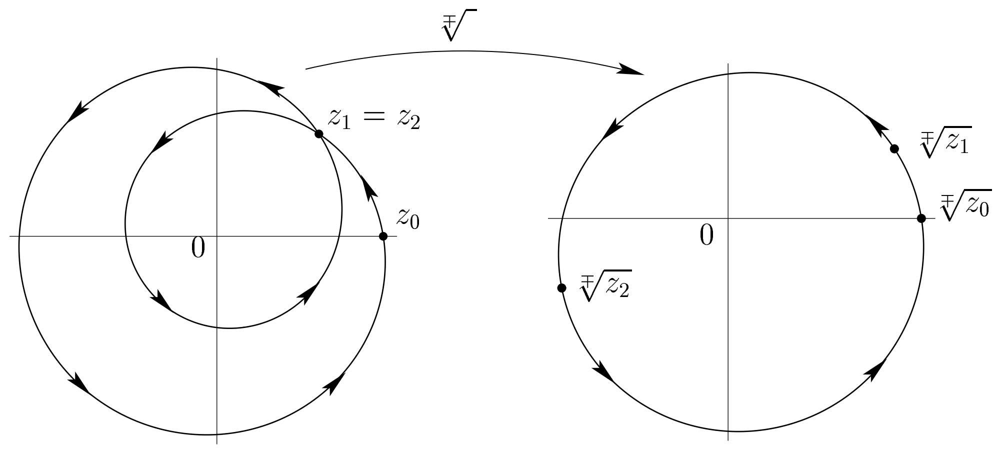

Figure 4: The image by the continuous square root of a continuous closed path winding twice around the origin is a continuous closed path winding once. Note that the point $z_1 = z_2$ that is met twice by the path, is mapped to two different values.

4.1 A square root without a branch cut

First we note that in all our calculations that present a potential branch cut problem, the square root is to be evaluated inside an integral along some path. It has therefore to be evaluated at points that are "close to each other". It is thus quite natural to define a *continuous square root* (that we denote by $\sqrt[\mp]{\ }$) along the path, in the following way: It has to remember the last result $\sqrt[\mp]{z_{n-1}}$ that it calculated; then to calculate the next value, it computes the usual square root $\sqrt{z_n}$, and chooses its sign $\sqrt[\mp]{z_n} = \pm\sqrt{z_n}$ so that $|\sqrt[\mp]{z_n} - \sqrt[\mp]{z_{n-1}}|$ is minimal.

We illustrate the result of evaluating the continuous square root along a path in figure 4, where the path is a closed curve winding twice around the origin; its image is a closed path that winds once around the origin. We see that the gain of avoiding the branch cut (and therefore defining a continuous function), is at the expense of the sign of the function not being globally defined.[5] Indeed, in our example we have $\sqrt[\mp]{z_1} \neq \sqrt[\mp]{z_2}$ although $z_1 = z_2$. Practically, the continuous square root is implemented by the following (schematized) code:

```
complex ∓√(complex z)
{
        static complex p = 0;
        complex w;

        w = √z;
        if (Re(w) Re(p) + Im(w) Im(p) < 0)
                w = −w;
        p = w;
        return w;
}
```

The variable p is declared "static", which means that its value is retained between two

[5]The domain of $\sqrt[\mp]{\ }$ should really be a double cover of $\mathbb{C} - \{0\}$; it would then be a well-defined holomorphic function.

calls of the function. The square root w is compared with the previous result p. If their "scalar product" $\mathrm{Re}(w)\,\mathrm{Re}(p) + \mathrm{Im}(w)\,\mathrm{Im}(p)$ is negative, we suspect that the branch cut was crossed, and thus we flip the sign of w.

We emphasize that the continuous square root makes sense only when it is evaluated along a path that does not meet the origin (practically, it has to be evaluated at successive values that are close to each other compared to their distance to the origin). We will thus only use it inside an integral and won't bother about the sign in front of the integral. Luckily, for the problems we need to solve, like (4.2), we will always be able to go around the fact that the global sign is ambiguous.

Finally, if the continuous square root is evaluated along a non-self-intersecting path that does not go through the origin, we can always draw a branch cut that does not meet the path. The holomorphic square root with this given branch cut is then equal (up to a global sign) to the continuous square root. The latter is therefore holomorphic in some neighborhood of the path.

4.2 Numerical evaluation of $\ell(z_i, z_j)$

Without loss of generality, we take $z_i = z_1$ and $z_j = z_2$. We need to numerically[6] evaluate

$$\ell(z_1, z_2) = \int_{z_1}^{z_2} \sqrt[\mp]{\phi(z)}dz = \int_{z_1}^{z_2} \frac{\sqrt[\mp]{-(z-z_1)(z-z_2)(z-z_3)(z-z_4)}}{z(z-1)(z-\xi)}dz\,, \tag{4.4}$$

where $z_1, \ldots, z_4$ are the four zeros of $\phi(z)$, and the integration is along a straight path. Parameterizing

$$z(t) = \frac{z_2 + z_1}{2} + \frac{z_2 - z_1}{2}t = z_1 + \frac{z_2 - z_1}{2}(t+1)\,, \tag{4.5}$$

we can rewrite this integral as

$$\ell(z_1, z_2) = \left(\frac{z_2 - z_1}{2}\right)^2 \int_{-1}^{1} \frac{\sqrt[\mp]{(z(t)-z_3)(z(t)-z_4)}}{z(t)(z(t)-1)(z(t)-\xi)}\sqrt{1-t^2}dt\,, \tag{4.6}$$

where we have written the usual square root $\sqrt{1-t^2}$; this is fine since $(1-t^2)$ is never negative on the integration path. But it is important to note here that we have made an arbitrary choice of sign in (4.6); indeed, since the global sign of the continuous square root is ambiguous, there is no way to tell which is the right sign in the identity $\sqrt[\mp]{xy} = \pm \sqrt[\mp]{x}\sqrt{y}$. But since we don't care about the global sign of $\ell(z_1, z_2)$, what sign we are choosing is not important, as long as we do the same choice of sign when computing $\frac{d}{da}\ell(z_i, z_j)$ (see (4.12) and comment thereafter).

We want to evaluate the integral (4.6) numerically. But we observe that, in general, one or more poles will be close enough to the path of integration to destroy the accuracy

[6] Putting aside the branch cut problem, the integral (4.4) can actually be expressed in terms of elliptic functions. We still compute it numerically for two reasons. First, the analytic expression is quite complicated, and since we have to evaluate it numerically anyway in order to solve (4.2), we wouldn't gain much. Second, (4.4) is integrable analytically only because the order of the polynomial in the square root is not greater than four (see for example [12]); and therefore an analytic evaluation of (4.4) would not generalize to contact interactions of order higher than four.

JHEP11(2004)018

of the numerical integration method. To remedy this, we subtract the finite poles from the integrand and add back the result of their analytic integrations:

$$\begin{aligned}\ell(z_1,z_2) \;=\; & \left(\frac{z_2-z_1}{2}\right)^2 \left\{\int_{-1}^{1}\left(\frac{\mp\sqrt{(z(t)-z_3)(z(t)-z_4)}}{z(t)(z(t)-1)(z(t)-\xi)} - \sum_{n=1}^{3}\frac{s_n r_n}{z(t)-p_n}\right)\sqrt{1-t^2}dt + \right.\\ & \left. +\sum_{n=1}^{3} s_n r_n \int_{-1}^{1}\frac{1}{z(t)-p_n}\sqrt{1-t^2}dt\right\}, \end{aligned} \tag{4.7}$$

where $p_1 = 0, p_2 = 1$ and $p_3 = \xi$ are the finite poles, and

$$r_n = \sqrt{(p_n-z_3)(p_n-z_4)}\prod_{\substack{m=1\\ m\neq n}}^{3}(p_n-p_m)^{-1}. \tag{4.8}$$

The signs $s_n = \pm 1$ are chosen in such a way that

$$\max_{t\in[-1,1]}\left\{\left|\frac{\mp\sqrt{(z(t)-z_3)(z(t)-z_4)}}{z(t)(z(t)-1)(z(t)-\xi)} - \sum_{n=1}^{3}\frac{s_n r_n}{z(t)-p_n}\right|\right\}$$

is minimal. For the four-point contact interaction, we have three finite poles and thus eight possible combinations of signs to try. Finally, we need the expression

$$\begin{aligned}\int_{-1}^{1}\frac{\sqrt{1-t^2}}{z(t)-p_n}dt &= \frac{2}{z_2-z_1}\int_{-1}^{1}\frac{\sqrt{1-t^2}}{t+q}dt\,, \qquad q=\frac{z_1+z_2-2p_n}{z_2-z_1}\\ &= \frac{2\pi}{z_2-z_1}\left(q - i\sqrt{1-q^2}\times\begin{cases}\mathrm{sgn}(\mathrm{Im\,q}) & \text{if } \mathrm{Im}\,q\neq 0\\ -\mathrm{sgn}(\mathrm{q}) & \text{if } \mathrm{Im}\,q = 0\end{cases}\right). \end{aligned} \tag{4.9}$$

Now that we have subtracted the poles, the integral

$$\int_{-1}^{1}\left(\frac{\mp\sqrt{(z(t)-z_3)(z(t)-z_4)}}{z(t)(z(t)-1)(z(t)-\xi)} - \sum_{n=1}^{3}\frac{s_n r_n}{z(t)-p_n}\right)\sqrt{1-t^2}dt \tag{4.10}$$

can be computed very precisely[7] with a Gauss method with weight $\sqrt{1-t^2}$ (Jacobi weight function) (see for example [13]). We use the method of rank 30 which, as we observe, has an accuracy of about twenty significant digits for $\xi = \frac{1}{2}+\frac{\sqrt{3}}{2}i$.

4.3 Numerical evaluation of $\frac{d}{da}\ell(z_i,z_j)$

Again, without loss of generality, we take $z_i = z_1$ and $z_j = z_2$. We have

$$\begin{aligned}\frac{d}{da}\ell(z_1,z_2) &= \frac{dz_2}{da}\mp\sqrt{\phi(z_2)} - \frac{dz_1}{da}\mp\sqrt{\phi(z_1)} + \int_{z_1}^{z_2}\frac{d}{da}\mp\sqrt{\phi(z)}\,dz\\ &= \int_{z_1}^{z_2}\frac{d}{da}\mp\sqrt{\phi(z)}\,dz\\ &= \frac{1}{2}\int_{z_1}^{z_2}\frac{1}{\mp\sqrt{\phi(z)}}\frac{1}{z(z-1)(z-\xi)}dz\,, \end{aligned} \tag{4.11}$$

[7]To avoid cancellation errors (subtracting two quantities that are large and close to each other), we should explicitly cancel the pole in (4.10). A simplified example is $\frac{\sqrt{t+1}}{t} - \frac{1}{t} = \frac{1}{\sqrt{t+1}+1}$, and the pole at $t=0$ has been explicitly cancelled. A similar simplification of the expression (4.10) is possible but it gives complicated expressions. Instead of doing that, our program always chooses the two independent paths that are the furthest away from the poles, so that the cancellation errors are not too large.

JHEP11(2004)018

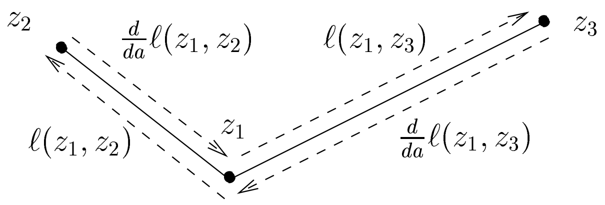

Figure 5: The arrows show the order in which the numerical integrations should be done. In order for the signs of the continuous square root to be consistent, the values used by the numerical integration methods should run continuously along the closed path formed by the arrows, starting and ending at z_1.

where we have used (2.4), and the fact that $\phi(z)$ vanishes at z_1 and z_2. Now we use again the parametrization (4.5), and we find

$$\frac{d}{da}\ell(z_1,z_2) = -\frac{1}{2}\int_1^{-1} \frac{1}{\mp\!\sqrt{(z(t)-z_3)(z(t)-z_4)}}\frac{dt}{\sqrt{1-t^2}}\,. \tag{4.12}$$

This integration[8] can be done numerically with a Gauss method with weight $1/\sqrt{1-t^2}$. We use here the method of rank 30.

It is important to note, as already mentioned after eq. (4.6), that we have made the same choices of signs in both the calculations of $\ell(z_1,z_2)$ and $\frac{d}{da}\ell(z_1,z_2)$, namely

$$\mp\!\sqrt{\phi(z(t))} = \frac{z_2-z_1}{2}\,\frac{\mp\!\sqrt{(z(t)-z_3)(z(t)-z_4)}}{z(t)(z(t)-1)(z(t)-\xi)}\sqrt{1-t^2}\,. \tag{4.13}$$

The relative signs of $\ell(z_1,z_2)$ and $\frac{d}{da}\ell(z_1,z_2)$ will therefore be consistent if the numerical integrations are done one after the other, and if the path of the second integral is the reverse path of the first one (see figure 5). This is why we have written the limits of integration in (4.12) in the opposite order as in (4.7). In this way, the continuous square root will be evaluated at successive points that are close to each other, and we will thus have avoided any branch cut problem.

We observe that if the initial value of a is not too far from the Strebel value, the Newton method converges to the Strebel solution.

5. Computation of the mapping radii

5.1 The finite poles

The mapping radius at the puncture p_n is given by ([10]):

$$\ln\rho_n = \lim_{\epsilon\to 0}\left(\mathrm{Im}\int_{p_n+\epsilon}^{\tilde z}\sqrt{\phi(z)}dz + \ln\epsilon\right), \tag{5.1}$$

[8] We are not subtracting the poles here. Indeed, the accuracy that we would gain would only make the Newton method slightly faster, without effecting the accuracy of the final result.

where $\tilde{z}$ is any point lying on the closest critical trajectory, ϵ is a positive real number, and the path of integration is chosen such that it avoids the branch cuts. Here we will take $\tilde{z}$ to be a zero, say z_1, that lies on the closest critical trajectory, and the path can be chosen to be a straight line if we replace the square root by the continuous square root. Moreover, since the residue of $\sqrt{\phi(z)}$ at $z = p_n$ is purely imaginary, (5.1) doesn't change if we replace the lower integration limit by $p_n + \epsilon\alpha$, where $|\alpha| = 1$. Thus

$$\ln \rho_n = \lim_{\epsilon\to 0} \left(\operatorname{Im} \int_{p_n+\epsilon\alpha}^{z_1} \mp\!\!\sqrt{\phi(z)}dz + \ln\epsilon \right) , \qquad \alpha = \frac{z_1 - p_n}{|z_1 - p_n|} , \tag{5.2}$$

and the sign of the continuous square root is chosen in such a way that the limit exists. The above expression is clearly very inconvenient for numerical evaluation. But we can remedy this by explicitly cancelling the singularity at $\epsilon = 0$. First, we note that

$$\lim_{\epsilon\to 0} \left(\ln\epsilon - \left(-\frac{1}{\sqrt{z_1 - p_n}} \int_{p_n+\epsilon\alpha}^{z_1} \frac{\sqrt{z_1 - z}}{z - p_n} dz + 2(\ln 2 - 1) + \ln|z_1 - p_n| \right) \right) = 0 . \tag{5.3}$$

And thus

$$\begin{aligned} \ln \rho_n &= \lim_{\epsilon\to 0} \left(\operatorname{Im} \int_{p_n+\epsilon\alpha}^{z_1} \left(\mp\!\!\sqrt{\phi(z)} - \frac{i}{\sqrt{z_1 - p_n}} \frac{\sqrt{z_1 - z}}{z - p_n} \right) dz \right) + 2(\ln 2 - 1) + \ln|z_1 - p_n| \\ &= \operatorname{Im} \int_{p_n}^{z_1} \left(\mp\!\!\sqrt{\phi(z)} - \frac{i}{\sqrt{z_1 - p_n}} \frac{\sqrt{z_1 - z}}{z - p_n} \right) dz + 2(\ln 2 - 1) + \ln|z_1 - p_n| . \end{aligned} \tag{5.4}$$

Thus

$$\begin{aligned} \rho_n &= \frac{4}{e^2}|z_1 - p_n| \times \\ &\times \exp\left(\operatorname{Im}\left\{ (z_1 - p_n) \int_0^1 \left(\frac{\mp\!\!\sqrt{-(p_n - z_1)(z - z_2)(z - z_3)(z - z_4)}}{z(z-1)(z-\xi)} - \frac{i}{z - p_n} \right) \sqrt{t}dt \right\} \right) , \end{aligned} \tag{5.5}$$

where we have parameterized $z = z_1 + t(p_n - z_1)$. The sign of the continuous square root is chosen so that the integrand is finite for $z \to p_n$. The integral is computed numerically with a rank 30 Gauss method with weight $\sqrt{t}$.

We haven't yet said how to know which zeros lie on the closest critical trajectory. One method would be to actually compute the critical trajectory, but this would require solving a differential equation, which can be hard numerically, and is certainly time consuming. Another method, that we are using here,[9] consists of calculating the radius for *all four* zeros z_i. One of the four results may be different from the other three, we discard it since it must correspond to the zero not lying on the closest critical trajectory. Practically, we discard the value that is the furthest away from the average value. The redundancy of calculations can then be used to evaluate the numerical errors affecting the mapping radii. If we denote by $\rho_n^{(i)}$ the mapping radius for the pole p_n calculated with the zero z_i, and if z_j is the discarded zero, we identify ρ_n with the average $\rho_n \approx \bar{\rho_n} = \frac{1}{3}\sum_{\substack{i=1\\i\neq j}}^4 \rho_n^{(i)}$. And we can estimate the variance of this sample $\sigma_{\rho_n}^2 \approx \frac{1}{2}\sum_{\substack{i=1\\i\neq j}}^4 (\rho_n^{(i)} - \bar{\rho_n})^2$.

[9]This particular method does not generalize to vertices of higher order. Indeed at order five we already have six zeros, and discarding three zeros out of them is thus impossible. For these higher vertices, we can use a fixed labelling of the zeros and poles and always make sure that the topology of the critical graph doesn't change, so that we always know which zeros are associated with which poles (see [14]).

JHEP11(2004)018

5.2 The pole at infinity

Here we must calculate the mapping radius in the coordinate $w = 1/z$, in which the pole is at $w = 0$. From $\phi(w)(dw)^2 = \phi(z)(dz)^2$ we have that $\phi(w) = \phi(z = 1/w)/w^4$. Thus

$$\begin{aligned}\ln \rho_4 &= \lim_{\epsilon \to 0} \left(\mathrm{Im} \int_{\epsilon\alpha}^{1/z_1} \mp\sqrt{\phi(w)}dw + \ln \epsilon \right), \qquad \alpha = \frac{z_1^*}{|z_1|} \\ &= \mathrm{Im} \int_0^{1/z_1} \left(\frac{\mp\sqrt{\phi(z = 1/w)}}{w^2} - i\frac{\sqrt{1 - wz_1}}{w} \right) dw + 2(\ln 2 - 1) - \ln |z_1| ,\end{aligned}$$

where z_1 is a zero that lies on the closest trajectory to the pole at infinity. With the parametrization $w = 1/z_1 - t/z_1$, we find

$$\rho_4 = \frac{4}{e^2|z_1|} \exp \left(\mathrm{Im} \left\{ \frac{1}{z_1} \int_0^1 \left(\frac{\mp\sqrt{-(1 - wz_2)(1 - wz_3)(1 - wz_4)}}{w(1 - w)(1 - w\xi)} - \frac{i}{w} \right) \sqrt{t}\, dt \right\} \right). \tag{5.6}$$

This expression is numerically calculated in the same way as (5.5).

6. The results as fits

The results obtained by our program are lengthy tables of data, namely the parameter a and the mapping radii ρ_n given at arbitrarily many points of the portion of moduli space $\mathcal{A}$. We do not write here any such table, but instead we express our results in the form of fits. Although some precision is lost with the fits, they are reasonably easy to use. The fits that we give below all have an error of the order of 0.1%, which should be precise enough for many calculations.

6.1 The boundary of the moduli space

The element $\mathcal{A}$ of moduli space that we are concentrating on, has $\mathrm{Re}\,\xi \leq 1/2$, $\mathrm{Im}\,\xi \geq 0$, and it is bounded by the unit circle centered at the origin, and by the curve $\mathcal{B}_1$ (see figure 3). To describe $\mathcal{A}$, we thus need to describe the part of $\mathcal{B}_1$ with $\mathrm{Re}\,\xi \leq 1/2$ and $\mathrm{Im}\,\xi \geq 0$, which we denote by $\tilde{\mathcal{B}}_1$. We parameterize this curve in terms of the angle θ (see figure 6), with the expression

$$\xi(\theta) = -r(\theta)\, e^{-i\theta} , \tag{6.1}$$

where $\theta \in [0, \theta_0]$, and $\theta_0 = 1.84644$ corresponds to the corner P with $\mathrm{Re}\,\xi = 1/2$. We will use the following fit

$$\xi^{\mathrm{fit}}(\theta) = -r^{\mathrm{fit}}(\theta)\, e^{-i\theta} , \tag{6.2}$$

where $r^{\mathrm{fit}}(\theta)$ is a polynomial of order five in θ

$$r^{\mathrm{fit}}(\theta) = 1 + \sum_{i=1}^{5} r_i\, \theta^i . \tag{6.3}$$

Note that the leading term has been set to one. In this way, the point $\xi = -1$, which we know is a corner of the moduli space (see section 3) and belongs to $\tilde{\mathcal{B}}_1$, will also belong to the fit of $\tilde{\mathcal{B}}_1$ (at $\theta = 0$); and the corner will be fitted properly.

JHEP11(2004)018

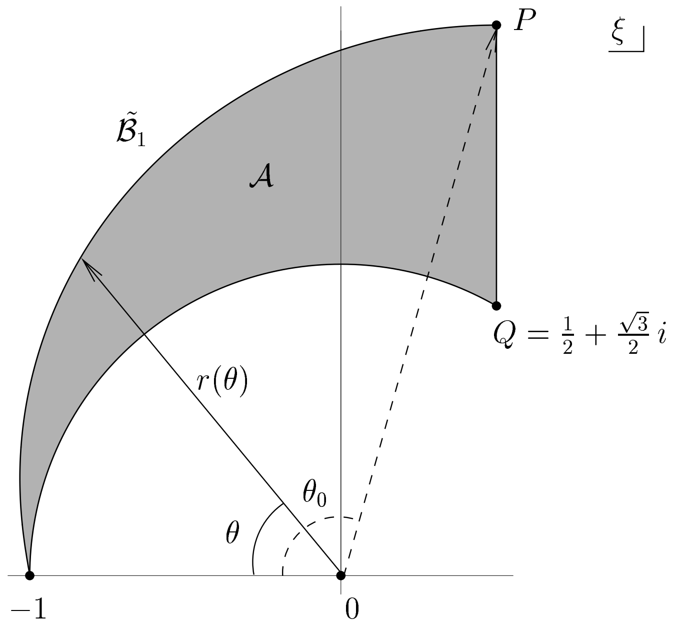

Figure 6: The parametrization of the curve $\tilde{\mathcal{B}}_1$ with the function $r(\theta)$.

The coefficients r_i in (6.3), are found by minimizing

$$\epsilon_r = \sqrt{\frac{\int_{\tilde{\mathcal{B}}_1} \left(r^{\rm fit}(\theta) - r(\theta)\right)^2 ds}{\int_{\tilde{\mathcal{B}}_1} ds}}\,. \tag{6.4}$$

Here ds is the length element; the denominator in the square root of (6.4) is thus the length of $\tilde{\mathcal{B}}_1$ and has been put there in order to normalize the error. We find

$$r^{\rm fit}(\theta) = 1 + 0.196639\,\theta + 0.264670\,\theta^2 - 0.130932\,\theta^3 + 0.062563\,\theta^4 - 0.015452\,\theta^5\,, \tag{6.5}$$

with error $\epsilon_r = 0.00022$. It is also useful to measure the maximum error made by this fit

$$\delta_r = \max_{\theta\in[0,\theta_0]} \left\{ \left| r^{\rm fit}(\theta) - r(\theta) \right| \right\} = 0.00088\,. \tag{6.6}$$

6.2 The Strebel differential

We write $\xi = x + y\,i$. And we use a polynomial fit of total order 5 in x and y

$$a^{\rm fit}(\xi) = \sum_{i+j\le 5} a_{ij}\, x^i y^j\,, \qquad \xi \in \mathcal{A}\,. \tag{6.7}$$

The coefficients a_{ij} are found by minimizing the error

$$\epsilon_a = \sqrt{\frac{\int_{\mathcal{A}} \left|a^{\rm fit}(\xi) - a(\xi)\right|^2 dxdy}{\int_{\mathcal{A}} dxdy}}\,. \tag{6.8}$$

We find

$$
\begin{aligned}
a^{\mathrm{fit}}(\xi) \;=\; & (0.67867 + 0.46345\,i) + (2.07710 + 0.49176\,i)\,x + (0.20000 + 0.58477\,i)\,y\, + \\
& + (1.61074 - 0.64246i)x^2 - (0.09194 - 0.36467i)xy + (0.05965 + 0.38101i)y^2 - \\
& - (0.33945 + 0.80519i)x^3 - (0.35448 - 0.94778i)x^2y - (1.04747 + 0.85263i)xy^2 + \\
& + (0.56049 - 0.43233i)y^3 - (0.63061 + 0.05352i)x^4 + (0.27490 + 0.76364i)x^3y - \\
& - (0.89712 + 0.75355i)x^2y^2 + (0.70167 + 0.46374i)xy^3 - (0.50743 - 0.12128i)y^4 - \\
& - (0.07990 - 0.08258i)x^5 + (0.32821 + 0.08618i)x^4y - (0.08918 + 0.20755i)x^3y^2 + \\
& + (0.37843 + 0.20916i)x^2y^3 - (0.15046 + 0.08495i)xy^4 + (0.11992 - 0.00719i)y^5
\end{aligned} \tag{6.9}
$$

with $\epsilon_a = 0.0011$. The maximum error made by this fit is

$$
\delta_a = \max_{\xi \in \mathcal{A}} \left\{ \left| a^{\mathrm{fit}}(\xi) - a(\xi) \right| \right\} = 0.0037\,. \tag{6.10}
$$

6.3 The mapping radii

We use again polynomials of order 5

$$
\rho_n^{\mathrm{fit}}(\xi) = \sum_{i+j \leq 5} \rho_{n,ij}\, x^i y^j\,, \tag{6.11}
$$

but here we minimize the average of the square of the *relative* errors

$$
\epsilon_{\rho_n} = \sqrt{\frac{\int_{\mathcal{A}} \left(\frac{\rho_n^{\mathrm{fit}}(\xi) - \rho_n(\xi)}{\rho_n(\xi)} \right)^2 dxdy}{\int_{\mathcal{A}} dxdy}}\,. \tag{6.12}
$$

This is more natural than the absolute error, because the mapping radii appear as a fundamentally multiplicative factor (see 2.6); in some sense, they measure the sizes of the images of the unit disks. The results of the fits are

$$
\begin{aligned}
\rho_1^{\mathrm{fit}}(\xi) \;=\; & 0.31883 + 0.14609x + 0.18216y + 0.47185x^2 + 0.14573xy + 0.15017y^2 + \\
& + 0.01342x^3 - 0.11152x^2y - 0.29992xy^2 + 0.02631y^3 - 0.15920x^4 + 0.01005x^3y - \\
& - 0.28574x^2y^2 + 0.17921xy^3 - 0.10879y^4 - 0.02838x^5 + 0.08245x^4y - \\
& - 0.01874x^3y^2 + 0.12423x^2y^3 - 0.03863xy^4 + 0.03250y^5\,, \qquad (6.13) \\
\rho_2^{\mathrm{fit}}(\xi) \;=\; & 0.78098 - 0.59124x + 0.17253y - 0.40055x^2 + 0.44703xy - 0.10848y^2 + \\
& + 0.10574x^3 + 0.27517x^2y - 0.03518xy^2 - 0.05091y^3 + 0.15196x^4 - 0.08497x^3y + \\
& + 0.05597x^2y^2 - 0.08168xy^3 + 0.07637y^4 + 0.01799x^5 - \\
& - 0.08381x^4y + 0.02112x^3y^2 - 0.05276x^2y^3 + 0.02554xy^4 - 0.01999y^5\,, \qquad (6.14) \\
\rho_3^{\mathrm{fit}}(\xi) \;=\; & 0.29797 - 0.36138x + 0.18030y + 0.17997x^2 + 0.49329xy + 0.32231y^2 - \\
& - 0.33706x^3 + 0.61497x^2y - 0.72821xy^2 + 0.23999y^3 - 0.16258x^4 + 0.41692x^3y - \\
& - 0.71139x^2y^2 + 0.46090xy^3 - 0.24944y^4 + 0.01369x^5 + 0.11153x^4y - \\
& - 0.13361x^3y^2 + 0.21281x^2y^3 - 0.10159xy^4 + 0.05898y^5\,, \qquad (6.15)
\end{aligned}
$$

JHEP11(2004)018

$$\rho_4^{\rm fit}(\xi) = 0.95136 + 0.48365x - 0.36818y - 0.16100x^2 - 0.52786xy - 0.01609y^2 - \\ - 0.20922x^3 + 0.00970x^2y + 0.19654xy^2 + 0.02470y^3 - 0.00082x^4 + 0.17750x^3y + \\ + 0.08937x^2y^2 - 0.01417xy^3 + 0.01641y^4 + 0.01554x^5 + 0.00976x^4y - \\ - 0.03639x^3y^2 - 0.03248x^2y^3 - 0.00411xy^4 - 0.00697y^5 \,. \tag{6.16}$$

The errors are respectively

$$\begin{aligned} \epsilon_{\rho_1} &= 0.00051 \\ \epsilon_{\rho_2} &= 0.00025 \\ \epsilon_{\rho_3} &= 0.00035 \\ \epsilon_{\rho_4} &= 0.00028 \,, \end{aligned} \tag{6.17}$$

while the maximum relative errors $\delta_{\rho_n} = \max_{\xi\in\mathcal{A}}\{|\rho_n^{\rm fit}(\xi) - \rho_n(\xi)|/\rho_n(\xi)\}$ are

$$\begin{aligned} \delta_{\rho_1} &= 0.0020 \\ \delta_{\rho_2} &= 0.0009 \\ \delta_{\rho_3} &= 0.0010 \\ \delta_{\rho_4} &= 0.0014 \,. \end{aligned} \tag{6.18}$$

7. The four-tachyon contact term

As en elementary check of our results, we compare the easiest quantity that is calculable from our data, namely the four-tachyon contact term, with a result previously obtained, with a different method, in [7]. It appears as the coefficient v_4 in the classical tachyonic potential

$$V(t) = -t^2 - \sum_{N=3}^{\infty} v_N \frac{t^N}{N!} \tag{7.1}$$

(note that this is not the effective potential, it is the potential of the tachyon when we ignore all other fields). The coefficients v_N are given by ([7], [10])

$$v_N = (-1)^N \frac{2}{\pi^{N-3}} \int_{\mathcal{V}_{0,N}} \left(\prod_{n=1}^{N-3} d^2\xi_n\right) \prod_{n=1}^{N} \rho_n^{-2} \,, \tag{7.2}$$

where $\mathcal{V}_{0,N}$ is the restricted moduli space of the N-punctured sphere, and ρ_n is the mapping radius at the puncture ξ_n. Thus

$$\begin{aligned} v_4 &= \frac{2}{\pi} \int_{\mathcal{V}_{0,4}} (\rho_1\rho_2\rho_3\rho_4)^{-2}\, d^2\xi \\ &= \frac{24}{\pi} \int_{\mathcal{A}} (\rho_1\rho_2\rho_3\rho_4)^{-2}\, d^2\xi \,, \end{aligned} \tag{7.3}$$

where we have used the fact that the measure $(\rho_1\rho_2\rho_3\rho_4)^{-2}\, d^2\xi$, is invariant under the action of $\mathrm{PSL}(2,\mathbb{C})$ transformations that permute the fixed poles $\{0, 1, \infty\}$, and under complex conjugation; the integration over $\mathcal{V}_{0,4}$ can thus be replaced by 12 times the integration over the twelfth of moduli space $\mathcal{A}$. Using our full data, we get

$$v_4 = 72.390 \pm 0.003\,, \tag{7.4}$$

in agreement with the result $v_4 = 72.39$ found in [7]. The uncertainty in (7.4) was computed from the uncertainties in the mapping radii (see Section 5), and the uncertainty from the numerical integration over $\mathcal{A}$, which was done with a Monte-Carlo technique.

It is also interesting to compare this to the same calculation done with the fits given in section 6. We obtain $v_4^{\rm fit} = 72.41$, less than 0.03% away from the value (7.4).

8. Conclusions

We have described numerically the geometry of the contact interaction of four off-shell closed bosonic string states. Our results give the Strebel differentials and the mapping radii everywhere in the twelfth of moduli space $\mathcal{A}$, from which we can extend the results to the whole moduli space $\mathcal{V}_{0,4}$ by straightforward $\mathrm{PSL}(2,\mathbb{C})$ transformations and complex conjugations. We have illustrated how the knowledge of the Strebel differentials and the mapping radii can be used to calculate the local coordinates around the punctures of the Riemann sphere. Our results can therefore be used to insert off-shell vertex operators on the four-punctured sphere, which is needed to compute off-shell contact amplitudes of four closed string states.

The numerical methods that we have developed can be generalized to contact interactions of more than four strings. Actually, the motivation for the present work was to compute the bulk tachyon potential and investigate whether it has a minimum or not. While the present paper doesn't offer any new information about the tachyon potential, it confirms its quartic term, previously calculated in [7] with a different method. A generalization of the work presented here, to quintic order in the string field, is in progress ([14]) and will hopefully give the tachyon potential to order five.

It would be interesting to use the results of this paper for doing concrete calculations in CSFT to quartic order in diverse backgrounds, for example in an orbifold background ([8, 9]). Another interesting application would be to do computations in heterotic string field theory ([15]).

Acknowledgments

I am indebted to Barton Zwiebach for many useful discussions. I also thank Yoji Michishita, Martin Schnabl and Peter West for useful conversations. And I would like to thank Jean-Pierre Derendinger and the Institute of Physics of the University of Neuchâtel, where part of this work was done, for their hospitality during the summer of 2003. This work has been supported in part by the Swiss National Science Foundation, and by the PPARC rolling grant: PPA/G/O/2002/00475.

References

[1] B. Zwiebach, *Closed string field theory: quantum action and the B-V master equation*, *Nucl. Phys.* **B 390** (1993) 33 [hep-th/9206084];
T. Kugo, H. Kunitomo and K. Suehiro, *Nonpolynomial closed string field theory*, *Phys. Lett.* **B 226** (1989) 48;
T. Kugo and K. Suehiro, *Nonpolynomial closed string field theory: action and its gauge invariance*, *Nucl. Phys.* **B 337** (1990) 434;
H. Sonoda and B. Zwiebach, *Covariant closed string theory cannot be cubic*, *Nucl. Phys.* **B 336** (1990) 185;
B. Zwiebach, *Quantum closed strings from minimal area*, *Mod. Phys. Lett.* **A 5** (1990) 2753;
M. Kaku, *Geometric derivation of string field theory from first principles: closed strings and modular invariance*, *Phys. Rev.* **D 38** (1988) 3052.

[2] M. Saadi and B. Zwiebach, *Closed string field theory from polyhedra*, *Ann. Phys. (NY)* **192** (1989) 213.

[3] B. Zwiebach, *Consistency of closed string polyhedra from minimal area*, *Phys. Lett.* **B 241** (1990) 343; *How covariant closed string theory solves a minimal area problem*, *Commun. Math. Phys.* **136** (1991) 83.

[4] P. West, *The spontaneous compactification of the closed bosonic string*, *Phys. Lett.* **B 548** (2002) 92 [hep-th/0208214].

[5] P.G.O. Freund, *Superstrings from twentysix-dimensions?*, *Phys. Lett.* **B 151** (1985) 387;
A. Casher, F. Englert, H. Nicolai and A. Taormina, *Consistent superstrings as solutions of the $d = 26$ bosonic string theory*, *Phys. Lett.* **B 162** (1985) 121;
F. Englert, H. Nicolai and A. Schellekens, *Superstrings from twentysix-dimensions*, *Nucl. Phys.* **B 274** (1986) 315;
F. Englert, L. Houart and A. Taormina, *The bosonic ancestor of closed and open fermionic strings*, hep-th/0203098;
A. Chattaraputi, F. Englert, L. Houart and A. Taormina, *Fermionic subspaces of the bosonic string*, *Class. and Quant. Grav.* **20** (2003) S449 [hep-th/0212085].

[6] V.A. Kostelecky and S. Samuel, *Collective physics in the closed bosonic string*, *Phys. Rev.* **D 42** (1990) 1289.

[7] A. Belopolsky, *Effective tachyonic potential in closed string field theory*, *Nucl. Phys.* **B 448** (1995) 245 [hep-th/9412106].

[8] A. Adams, J. Polchinski and E. Silverstein, *Don't panic! closed string tachyons in ALE space-times*, *J. High Energy Phys.* **10** (2001) 029 [hep-th/0108075];
J.A. Harvey, D. Kutasov, E.J. Martinec and G.W. Moore, *Localized tachyons and rg flows*, hep-th/0111154;
C. Vafa, *Mirror symmetry and closed string tachyon condensation*, hep-th/0111051;
R. Gregory and J.A. Harvey, *Spacetime decay of cones at strong coupling*, *Class. and Quant. Grav.* **20** (2003) L231 [hep-th/0306146];
A. Dabholkar, *On condensation of closed-string tachyons*, *Nucl. Phys.* **B 639** (2002) 331 [hep-th/0109019];
Y.H. He, *Closed string tachyons, non-supersymmetric orbifolds and generalised McKay correspondence*, *Adv. Theor. Math. Phys.* **7** (2003) 121 [hep-th/0301162];
S. Sarkar and B. Sathiapalan, *Closed string tachyons on $C/Z(n)$*, hep-th/0309029;

M. Headrick, *Decay of $C/Z(n)$: exact supergravity solutions*, *J. High Energy Phys.* **03** (2004) 025 [hep-th/0312213];
A. Dabholkar, A. Iqubal and J. Raeymaekers, *Off-shell interactions for closed-string tachyons*, *J. High Energy Phys.* **05** (2004) 051 [hep-th/0403238];
M. Headrick, S. Minwalla and T. Takayanagi, *Closed string tachyon condensation: an overview*, *Class. and Quant. Grav.* **21** (2004) S1539 [hep-th/0405064];
T. Sarkar, *On localized tachyon condensation in $C^2/Z(n)$ and $C^3/Z(n)$*, *Nucl. Phys.* **B 700** (2004) 490 [hep-th/0407070].

[9] Y. Okawa and B. Zwiebach, *Twisted tachyon condensation in closed string field theory*, *J. High Energy Phys.* **03** (2004) 056 [hep-th/0403051].

[10] A. Belopolsky and B. Zwiebach, *Off-shell closed string amplitudes: towards a computation of the tachyon potential*, *Nucl. Phys.* **B 442** (1995) 494 [hep-th/9409015].

[11] K. Strebel, *Quadratic differentials*, Springer Verlag, 1984.

[12] I.S. Gradshteyn and I.M. Ryzhik, *Table of integrals, series, and products*, Academic Press, Fifth Edition, 1994;
P.F. Byrd and M.D. Friedman *Handbook of elliptic integrals for engineers ans scientists*, Springer Verlag, Second Edition, 1971.

[13] A. Ralston and P. Rabinowitz, *A first course in numerical analysis*, McGraw-Hill, 1978, second Edition.

[14] N. Moeller, *Closed bosonic string field theory at quintic order*, to appear.

[15] Y. Okawa and B. Zwiebach, *Heterotic string field theory*, *J. High Energy Phys.* **07** (2004) 042 [hep-th/0406212].